

# 35 nm- $L_g$ Raised S/D In<sub>0.53</sub>Ga<sub>0.47</sub>As Quantum-well MOSFETs with 81 mV/decade Subthreshold Swing at $V_{DS}=0.5$ V

Sanghoon Lee<sup>1</sup>, Cheng-Ying Huang<sup>1</sup>, Doron C. Elias<sup>1</sup>, Brian J. Thibeault<sup>1</sup>, William Mitchell<sup>1</sup>, Varistha Chobpattana<sup>2</sup>, Susanne Stemmer<sup>2</sup>, Arthur C. Gossard<sup>2</sup>, and Mark J. W. Rodwell<sup>1</sup>

<sup>1</sup>ECE Department, <sup>2</sup>Materials Department, University of California, Santa Barbara, CA 93106-9560  
Phone: 805-452-2920, Fax: 805-893-3262, Email: sanghoon\_lee@ece.ucsb.edu

Recently, InAs or In-rich InGaAs (In>53%) has been widely studied as the channel material for III-V FETs due to its superior electron transport properties over In<sub>0.53</sub>Ga<sub>0.47</sub>As. These materials provide excellent on-state characteristics, e.g. >2.5 mS/ $\mu$ m peak transconductance ( $g_m$ ) at  $V_{DS}=0.5$  V [1-3]. The narrow bandgap in these materials, however, causes band-to-band tunneling (BTBT) in the high drain-field region even at relatively low supply voltage of 0.5 V, thus resulting in high leakage at the off-state [1][3]. In our previous work, in order to address this issue, we incorporated a vertical spacer between the channel and N<sup>+</sup> source/drain (S/D) to accommodate the depletion region near the channel-drain junction. The spacer significantly improved off-state characteristics such as off-state leakage, drain-induced barrier lowering (DIBL), and subthreshold swing (SS) without increasing the device footprint [3], [4]. In this work, by adopting a ~4 nm-thick In<sub>0.53</sub>Ga<sub>0.47</sub>As channel instead of a thick InAs channel, we have further improved the off-state characteristics at high  $V_{DS}$  and achieved 81 mV/dec. minimum subthreshold swing (SS<sub>min</sub>) for a 35 nm- $L_g$  device at  $V_{DS}=0.5$  V and 385  $\mu$ A/ $\mu$ m on-current ( $I_{on}$ ) at 100 nA/ $\mu$ m off-current ( $I_{off}$ ) and  $V_{DD}=0.5$  V, which are the best SS<sub>min</sub> and  $I_{on}$  from all reported In<sub>0.53</sub>Ga<sub>0.47</sub>As channel FETs.

The epitaxial layers, grown on semi-insulating InP by solid source MBE, consist of a 7 nm unintentionally doped (U.I.D) In<sub>0.53</sub>Ga<sub>0.47</sub>As channel on an In<sub>0.52</sub>Al<sub>0.48</sub>As back-barrier, the details of which are described in [3]. ~50 nm of HSQ was spun and patterned by e-beam lithography for dummy gate formation. To form the vertical spacer and N<sup>+</sup> S/D, a 10 nm unintentionally doped and a 60 nm Si-doped ( $4 \cdot 10^{19} \text{ cm}^{-3}$ ) In<sub>0.53</sub>Ga<sub>0.47</sub>As layer were selectively regrown at 600°C using a MOCVD. Device mesas were isolated by a wet-etch. Dummy gates were removed in buffered oxide etch. To remove the surface which reacted with the dummy gates during the regrowth, ~3 nm of InGaAs surface was isotropically wet-etched using a digital etch [5]. The sample was then immediately loaded into an ALD. After *in-situ* N<sub>2</sub>/TMA treatment during which ~0.5 nm of Al<sub>2</sub>ON<sub>x</sub> was formed, ~3 nm HfO<sub>2</sub> was deposited [6]. The sample was then annealed in forming gas at 400°C. Ni/Au gate metals and Ti/Pd/Au S/D metal contacts were lifted-off using a thermal and an e-beam evaporator, respectively. The summary of the process flow and the cross-sectional schematic of the device structure are described in Fig. 1 (a) and (b). Fig. 1(c) shows a top-down SEM image for a device with a 35 nm of gate length ( $L_g$ ). Here, the  $L_g$  is defined as the spacing between the edges of the regrown layer. Because the vertical spacer is also gated as shown in Fig. 1(b), the effective gate length is ~34 nm larger than the lateral, lithographic gate length  $L_g$ .

Fig. 2 shows the transfer characteristics of a device with a 35 nm- $L_g$ . The device shows 1.7 mS/ $\mu$ m peak  $g_m$  at  $V_{DS}=0.5$  V and 385  $\mu$ A/ $\mu$ m on-current ( $I_{on}$ ) at a fixed  $I_{off}=100$  nA/ $\mu$ m and  $V_{DD}=0.5$  V. Fig. 3 shows the subthreshold characteristics for the 35 nm- $L_g$  device. Its SS<sub>min</sub> at  $V_{DS}=0.1$  and 0.5 V are 73 mV/dec. and 81 mV/dec., respectively. Its threshold voltage ( $V_T$ ) defined at  $I_D=1$   $\mu$ A/ $\mu$ m is 0.15 V, and DIBL is 85 mV/V. Fig. 4 shows the output characteristics of the 35 nm- $L_g$  device. The device exhibits excellent  $I_D$  saturation even at the short gate length. Its on-resistance ( $R_{on}$ ) is 304  $\Omega \cdot \mu$ m at  $V_{GS}=1.2$  V. Fig. 5 shows subthreshold characteristics of a device with a 1  $\mu$ m- $L_g$ . Its SS<sub>min</sub> at low  $V_{DS}$  of 0.1 V is 64 mV/dec., from which an interfacial trap density ( $D_{it}$ ) of  $2.8 \cdot 10^{12} \text{ cm}^{-2} \text{ eV}^{-1}$  is calculated. The gate leakage is negligible at all measured bias (not shown). Fig. 6 shows the peak  $g_m$  at  $V_{DS}=0.5$  V as a function of the gate length. The peak  $g_m$  does not saturate at 35 nm gate length, indicating that further gate length scaling may continue to improve on-state performance. Fig. 7 shows  $R_{on}$  as a function of gate length. The  $R_{on}$  extrapolated at the zero gate length is 233  $\Omega \cdot \mu$ m, which includes ~90  $\Omega \cdot \mu$ m S/D access resistance, as determined by TLM measurement (not shown). Fig. 8 shows DIBL as a function of the gate length, comparing with recently reported III-V MOSFETs. The devices in this work show significantly lower DIBL at similar gate lengths than other planar III-V MOSFETs. We believe that this is mostly because the vertical spacer and the thin 4nm channel improve electrostatic integrity especially at short  $L_g$ . In addition, the smaller off-state leakage at  $V_{DS}=0.5$  V of the In<sub>0.53</sub>Ga<sub>0.47</sub>As-channel MOSFETs, compared to that of InAs [3], is likely due to reduced BTBT in the high drain-field region. Fig. 9 shows SS<sub>min</sub> at  $V_{DS}=0.5$  V as a function of the gate length. These devices have the lowest SS<sub>min</sub> compared to any other III-V MOSFETs regardless of the device architecture, which is attributed to both the high-k dielectric with sub-1 nm EOT and low  $D_{it}$  and the design features mentioned above. Fig. 10 compares  $I_{on}$  at  $I_{off}=100$  nA/ $\mu$ m and  $V_{DD}=0.5$  V with recently reported III-V MOSFETs result. Due to the outstanding subthreshold characteristics, the devices have higher  $I_{on}$  at sub-50 nm- $L_g$  than other reported III-V MOSFETs.

[1] J. Lin, *et al.*, IEDM (2013), [2] S. W. Chang, *et al.*, IEDM (2013), [3] S. Lee, *et al.*, APL, vol. 103, no. 23 (2013), [4] S. Lee, *et al.*, EDL submitted, [5] S. Lee, *et al.* IPRM (2013), [6] V. Chobpattana, *et al.*, APL, vol. 113, (2013)

Acknowledgements: This research was supported by the SRC Non-classical CMOS Research Center (Task 1437.009). A portion of this work was done in the UCSB nanofabrication facility, part of NSF funded NNIN network.

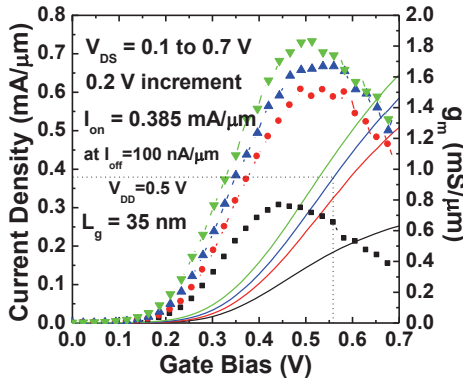
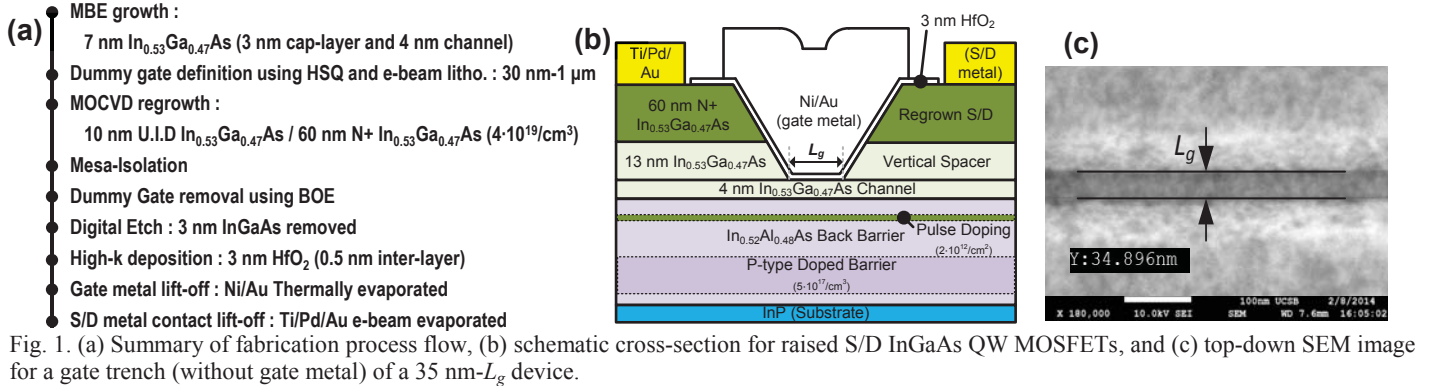


Fig. 2.  $I_D$ - $V_{GS}$  and  $g_m$  for a 35 nm- $L_g$  device.

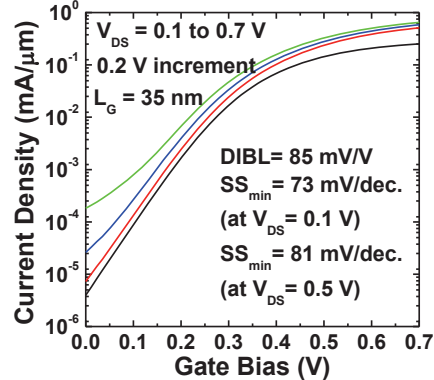


Fig. 3. log( $I_D$ )- $V_{GS}$  for a 35 nm- $L_g$  device.

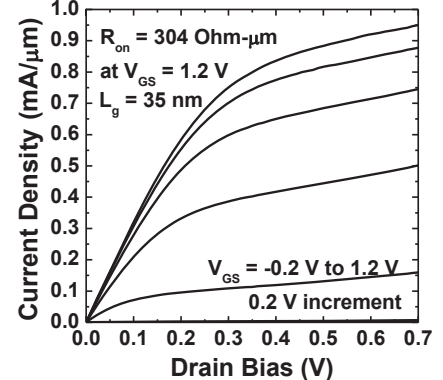


Fig. 4.  $I_D$ - $V_{DS}$  for a 35 nm- $L_g$  device.

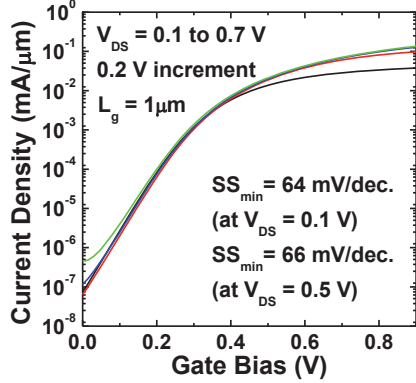


Fig. 5. log( $I_D$ )- $V_{GS}$  for a 1 μm- $L_g$  device.

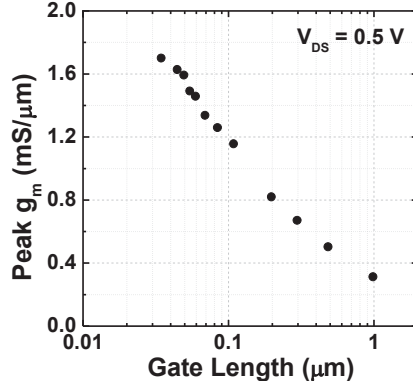


Fig. 6. Peak  $g_m$  vs.  $L_g$ .

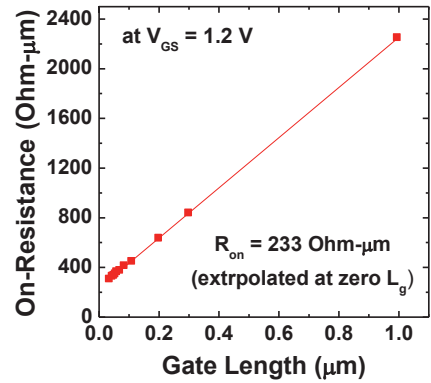


Fig. 7.  $R_{on}$  at  $V_{GS}=1.2$  V vs.  $L_g$ .

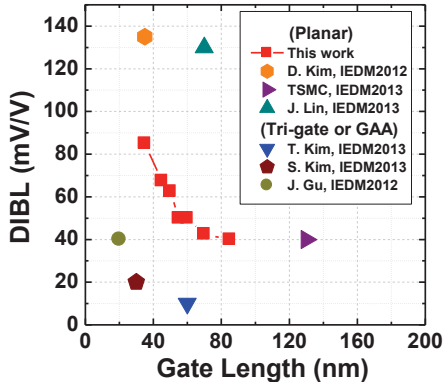


Fig. 8. DIBL vs.  $L_g$ , comparing with recently reported III-V MOSFETs

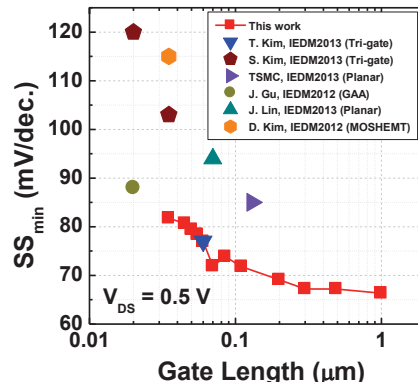


Fig. 9. SS<sub>min</sub> at  $V_{DS}=0.5$  V vs.  $L_g$ , comparing with recently reported III-V MOSFETs

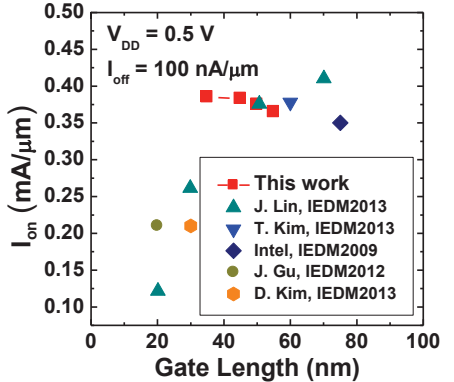


Fig. 10.  $I_{on}$  at  $I_{off}=100$  nA/μm and  $V_{DD}=0.5$  V vs.  $L_g$ , comparing with recently reported III-V MOSFETs